JOURNAL OF APPLIED ELECTROCHEMISTRY 16 (1986) 947–963

Electrochemical study of liquid–solid mass transfer in packed bed electrodes with upward and downward co-current gas–liquid flow

A. STORCK, M. A. LATIFI, G. BARTHOLE*, A. LAURENT, J. C. CHARPENTIER

Laboratoire des Sciences du Génie Chimique, CNRS–ENSIC, 1 rue Grandville, 54042 Nancy Cedex, France

Received 7 October 1985; revised 19 February 1986

Hydrodynamic and mass transfer parameters (pressure drop, gas and liquid hold-up, liquid–solid mass transfer coefficients) have been measured for porous electrodes with upward or downward co-current gas–liquid flow by means of several electrochemical techniques. The influence of the most important parameters (packing diameter, gas and liquid flow rates) and of the hydrodynamic flow regimes, has been studied. It is found that in the trickle flow regime the limiting current densities depend only on the liquid flow rates (with no measurable influence of the gas). In the upward flow configuration, the strong turbulence generated by the ascending gas bubbles leads to a sharp increase of current densities with the gas flow rate. A comparison between both configurations is presented.

Nomenclature

A_c	active electrode packing area
A_{eg}	geometrical electrode packing area
a_s	specific surface area of particle
a_v	specific surface area of packing
c_s	bulk concentration of reactive species
d_p	particle diameter
D	dispersion coefficient
D_L	diffusion coefficient of reacting species in the liquid phase
f	ratio of mass transfer coefficient with and without gas bubbles
F	Faraday constant
G	superficial mass velocity of gas
I	electric current
I_L	limiting electrolysis current
i	current density
J_D	Chilton–Colburn factor
k_d	true liquid to particle mass transfer coefficient
k'_{d0}	apparent liquid to particle mass transfer coefficient without gas bubble
k'_d	apparent liquid to particle mass transfer coefficient with gas bubble ($k'_d = k_d\phi$)
L	superficial mass velocity of liquid
Re	Reynolds number
R_e	equivalent resistance of electrolyte
R_{e0}	equivalent resistance of electrolyte without gas
Sc	Schmidt number
Sh	Sherwood number
t, t', t_1, t_2	time
t_s	mean residence time
U_c	cell voltage
U_0	cell voltage at equilibrium
u'_L	liquid interstitial velocity
u_{GO}	gas superficial linear velocity
u_{LO}	liquid superficial linear velocity
Z	distance between the two detectors
β	hold-up
$\Delta H/\Delta Z$	pressure drop per unit packing height

* *Present address*: Rhône–Poulenc Recherches, 14 rue des Gardinoux, 93308 Aubervilliers Cedex, France.

0021–891X/86 $03.00 + .12

ε	bed porosity
η_a	anodic overpotential
η_c	cathodic overpotential
λ	flow parameter, defined in Equation 6
μ	dynamic viscosity
ν	kinematic viscosity
ϱ	density
σ	surface tension
ϕ	fraction of particle area wetted by liquid
ψ	flow parameter defined in Equation 7

Subscripts

air	air
G	gas
L	liquid
t	total
W	water

1. Introduction

For several years a considerable interest has been directed towards the porous percolating electrode, PPE (granular porous electrodes or grids crossed by a forced flow of electrolyte). This type of structure involves high electrode area per unit volume of reactor and high overall mass transfer coefficient compared with classical equipment using plate electrodes [1, 2]. A number of experimental and theoretical studies have been published in the last 10 years on the topic of single liquid flow. As reported by Alkire and Ng [3], the potential applications are numerous and various, i.e. electrical energy storage, recovery of metals from dilute solutions and electro-organic synthesis. Fixed bed electrodes with simultaneous flow of gas and electrolyte solution have also been investigated for electrochemical processes involving gaseous reactants (O_2, SO_2, CO_2, NO, Cl_2, etc.). In this case, absorption of the gas into the liquid phase and further electrochemical reduction or oxidation of the dissolved gas take place simultaneously. Such 'trickle bed electrochemical reactors' (with downward co-current flow) have been studied extensively for hydrogen peroxide production by electroreduction of oxygen [4–6], for sodium dithionite production by cathodic reduction of sulphur dioxide [6] and for hydroxylamine production by electroreduction of nitric oxide [7]. The effects of current density, gas pressure and flow rate, electrolyte concentration and flow rate and bed geometry have been investigated. More recently, an electrochemical absorption device for gas purification (with countercurrent flow of gas and liquid) has been proposed by Kreysa *et al.* [8] and applied to chlorine and sulphur dioxide treatment.

For these processes where absorption with further electrochemical reaction occurs, the overall rate may depend either on the physical gas–liquid mass transfer parameters or on the liquid to particle mass transfer coefficient. Under certain operating conditions (where the concentrations of the dissolved gas is low), the process is limited by diffusional mass transfer resistance near the liquid–solid interface. The effect of gas flow through three-dimensional electrodes has received little attention from the viewpoint of mass transfer rates [9]. However, it is well known that gas sparging can greatly enhance the limiting current density while maintaining low pressure drop through parallel plate electrochemical reactors, for example. This subject has been recently treated by Economou and Alkire [10], as well as several authors [11–13] previously.

The present work concerns the determination of the overall mass transfer rate for a packing of conducting particles located inside a column operated in co-current gas–liquid flow using an electrochemical method. Two configurations are considered:

(i) upward co-current flow; in this case, the liquid is the continuous phase and the gas the dispersed one

(ii) downward co-current flow (referred to as 'trickle flow'), where the gas is the continuous phase.

In order to correlate the mass transfer results to hydrodynamic parameters the following factors are also considered:

(a) hydrodynamic flow regime and pressure loss

(b) gas and liquid hold-up inside the reactor. These parameters have been deduced by electrochemical methods based on electrolyte resistance measurement for the gas hold-up and on the

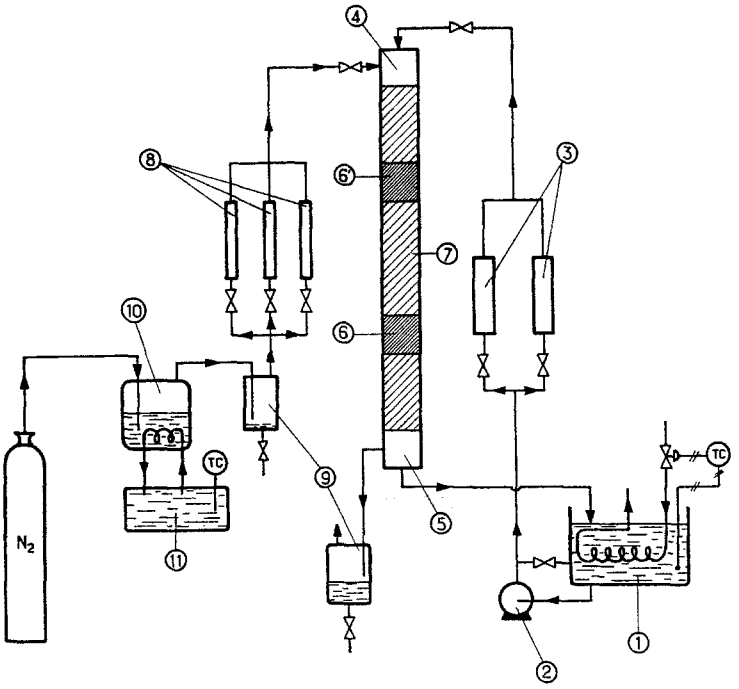

Fig. 1. Schematic view of the apparatus (downward co-current flow). 1, Storage tank; 2, centrifugal pump; 3, 8, rotameters; 4, gas–liquid distributor; 5, gas–liquid settler; 6, 6′, working electrodes; 7, sections of non-conducting particles; 9, gas–liquid separators; 10, gas saturator; 11, constant temperature bath.

classical residence time distribution determination for the liquid hold-up.

2. Apparatus and techniques

2.1. *Apparatus*

The equipment is schematically presented in Fig. 1 for the reactor operated with co-current downward gas liquid flow (for the upward configuration, the apparatus is similar and has been described elsewhere [14]). The glass column of length 1.30 m and inside diameter 50 mm was packed with 4-mm or 1-mm glass spheres with a porosity of 0.37 or 0.42, respectively.

Two active sections located respectively at 33 cm and 66 cm above the bottom of the column have been used for the determination of the mass transfer coefficient. Each of these consisted of 4-mm or 1-mm nickel sphere packing (height, 15 mm and 5 mm), a fine grid (made of a non-conducting material) which provided an electrical insulation between the packing, and the counter electrode (anode) which consisted of a nickel cylinder, 9 cm long, having the same diameter as the column. The anode–cathode system and a reference electrode (small platinum wire located near the working electrode) were incorporated in a classical three-electrode potentiostatic circuit including a TACUSSEL PRT 20-2 potentiostat and a Sefram current–potential curve recorder.

The electrolytic solution, maintained at 30° C, was a mixture of approximately 1.3×10^{-3} M ferricyanide ions and 0.1 M ferrocyanide ions in 0.5 M sodium hydroxide as supporting electrolyte. The experimental values obtained at 30° C for the electrolyte kinematic viscosity, ν_L, specific density, ϱ_L, and diffusion coefficient, D_L, of the ferricyanide ions were $0.91 \times 10^{-6}\,m^2\,s^{-1}$, $1021\,kg\,m^{-3}$ and $8.8 \times 10^{-10}\,m^2\,s^{-1}$, respectively. The dynamic viscosity, μ_G, of the gas (nitrogen) was 1.75×10^{-5} Pa s and its specific gravity, ϱ_G, was between 1.16 and $1.6\,kg\,m^{-3}$ depending on the pressure inside the column.

2.2. *Experimental techniques*

2.2.1. Pressure drop. The static pressure gradients, $\Delta H/\Delta Z$, of the gas–liquid mixture were measured by means of two pressure gauges located at the entrance and exit of the column.

2.2.2. Liquid to particle mass transfer coefficients. These were deduced from the limiting current obtained in the electrochemical reduction of the ferricyanide ions through the classical relation

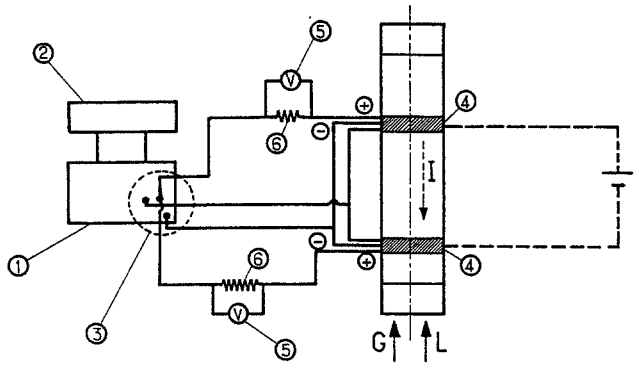

Fig. 2. Principle of the electrochemical measurements. 1, Potentiostat; 2, pilot; 3, electrodes; 4, active sections; 5, recording instrument; 6, resistances.

$$I_L = v_e F k_d A_e C_s$$

It should be mentioned that for a gas–liquid system the active electrode packing area, A_e, may be different from the geometrical area, A_{eg}, due to incomplete wetting of the particles, particularly for the trickle bed configuration where the gas is the continuous phase. Therefore, an apparent mass transfer coefficient is defined

$$k'_d = \frac{k_d A_e}{A_{eg}} = k_d \phi \qquad (1)$$

where $\phi = A_e/A_{eg}$ is the fraction of the particle area wetted by the liquid. Fig. 2 presents the electrical circuit used for the determination.

2.2.3. Gas hold-up (β_G). The principle of this measurement was also based on an electrochemical method. This involved the determination of an experimental plot of current density against voltage (U_c) in a cell where the anode and the cathode were the two conducting packings of nickel particles, located at a distance of 33 cm from each other (the oxidation of $Fe(CN)_6^{4-}$ and reduction of $Fe(CN)_6^{3-}$ were the two reactions involved and therefore $U_0 = 0$). By considering only the linear part of this curve and taking into consideration the fact that the equivalent resistance, R_e, of the electrolyte is high (due to the large distance between anode and cathode) and that, for the system $Fe(CN)_6^{3-}/Fe(CN)_6^{4-}$, the overpotentials η_a and η_c are low (particularly near the thermodynamic equilibrium), it follows as a first approximation that

$$U_c \simeq R_e I$$

The slope of the curve of U_c versus I thus gives R_e. The same procedure performed without gas allows the determination of the corresponding value, R_{e0}.

The ratio R_e/R_{e0} can be related to the gas hold-up, β_G, through various relationships proposed by several authors (Table 1) and reviewed recently by Hine [15]. (For $\beta_G < 0.4$, the difference between these relations is not significant.) It should be mentioned that this method is applicable only in the case where the gas is the dispersed phase (upward co-current flow) and also in conditions where the dispersion is homogeneous (no channelling, no pulsing flow, etc.).

2.2.4. Overall liquid hold-up (β_t). The residence time distribution of the liquid phase (cf. Fig. 3) inside the column [16] was determined by injection of a tracer (ferricyanide ions in sodium hydroxide) at the inlet of the cell. The two active sections (also used for the determination of the mass transfer rates), each of them operated potentiostatically at a sufficient negative potential, yield the signal $I'(0, t) = I(0, t) - I_0(0)$ and $I'(Z, t) = I(Z, t) - I_0(Z)$ proportional to the concentration of the tracer (under limiting

Table 1. Different correlations for determining the gas hold-up β_G from ratio Re/Re_0 [15]

Authors	*Re/Re_0*
Bruggeman	$(1 - \beta_G)^{-\frac{1}{2}}$
Rayleigh	$(1 + \beta_G)/(1 - \beta_G)$
Maxwell	$(1 + \beta_G/2)/(1 - \beta_G)$
Neale	$(3 - \beta_G)/2\beta_G$

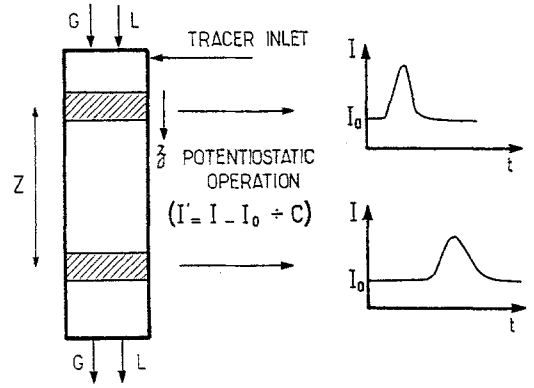

Fig. 3. Principle of the electrochemical 'residence time distribution' method.

current conditions. $I'(0, t)$ and $I'(Z, t)$ are related by the following relation [16]:

$$I'(Z, t) = \int_0^t I'(0, t)E(t - t')\,dt' \quad (2)$$

where $E(t)$ is the residence time distribution function.

In the Laplace domain, this relation becomes

$$Y(s) = G(s)X(s) \quad (3)$$

where $X(s)$, $Y(s)$ and $G(s)$ denote the Laplace transform of $I'(0, t)$, $I'(Z, t)$ and $E(t)$, respectively.

The mean residence time, t_s, is given by the difference $t_2 - t_1$ between the first order moments of $I'(Z, t)$ and $I'(0, t)$ and is related to β_t by

$$\beta_t = \frac{t_s u_{LO}}{\varepsilon Z} \quad (4)$$

3. Experimental results for the upward co-current gas–liquid flow

3.1. *Flow regimes*

For co-current upflow through a packed bed,

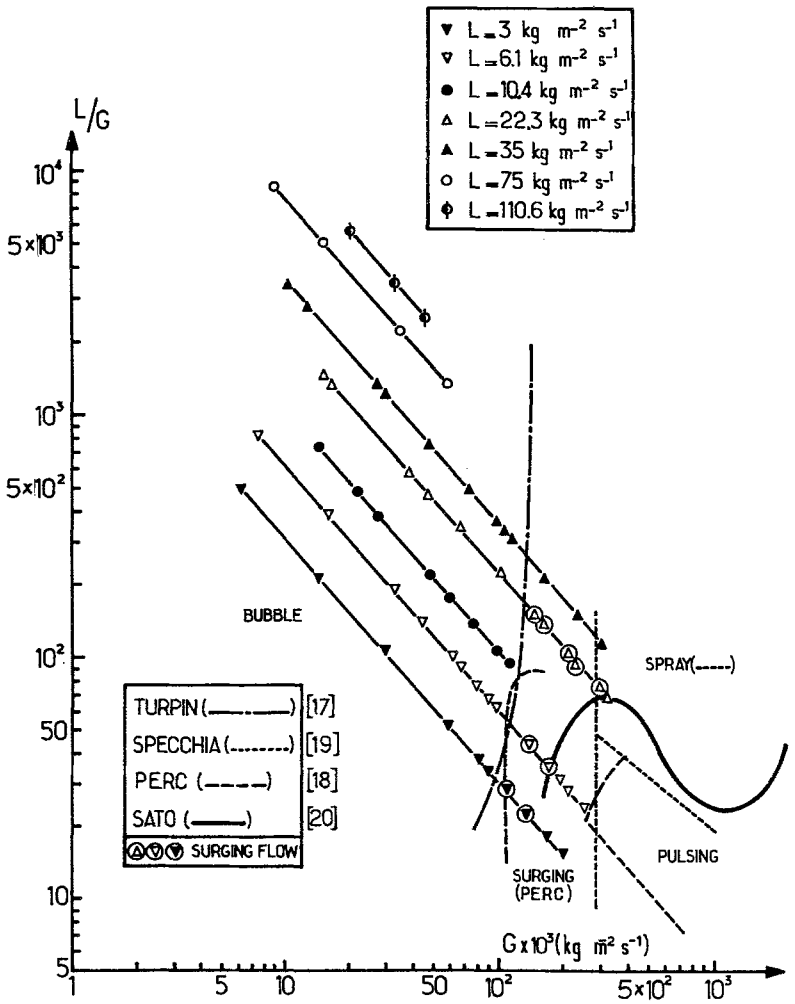

Fig. 4. Hydrodynamic regions observed for the upward co-current gas–liquid flow when d_p = 4 mm. Comparison with other works [17–20].

various flow regimes such as bubble flow (liquid continuous), surging flow, pulsed flow and spray flow (gas continuous) can be obtained depending on the gas and liquid flow rates and the nature and size of the packing [17–20]. The flow regime boundaries in terms of L/G versus G for the present data and for those reported in the literature are shown in Fig. 4. For the range of flow rates in our experiments, a visual observation has revealed three flow configurations, i.e. bubble, surging and pulsed flows. The flow boundaries presented in Fig. 4 are different for each of the various literature sources. However, our results are in good agreement with those of Turpin and Huntington [17] and the PERC [18] for the transition between bubble and pulsed flow. The different boundaries observed are attributable to the shape, size and wetting characteristics of the particles and the visual appreciation error. Most of our mass transfer results were obtained in the bubble flow regime and the electrochemical techniques used in this work cannot be applied in spray flow or even in conditions where the gas hold-up is too high.

3.2. *Gas hold-up*

As an example, the experimental variations of the gas hold-up, β_G, with the gas superficial velocity, u_{GO}, are reported in Fig. 5 for $L = 6\,kg\,m^{-2}\,s^{-1}$ and compared to the results of different authors [17, 20–24] whose experimental conditions are given in Table 2.

Examination of these figures and of Fig. 7 presenting the influence of the liquid flow rate, L, leads to the following conclusions.

(a) Except for the work of Sato *et al.* [20] and Fukushima and Kusaka [24], which correspond to higher particle diameter and smaller gas hold-up, the agreement between the different correlations and the present results is satisfactory.

(b) The best agreement is obtained by comparing our results to the correlation deduced by Achwal and Stepanek [22], whose method was based on the measurement of the electrical conductivity of the liquid. For L ranging from 4 to $70\,kg\,m^{-2}\,s^{-1}$ and G ranging from 7×10^{-3} to $0.6\,kg\,m^{-2}\,s^{-1}$, they proposed the following relationship for β_G:

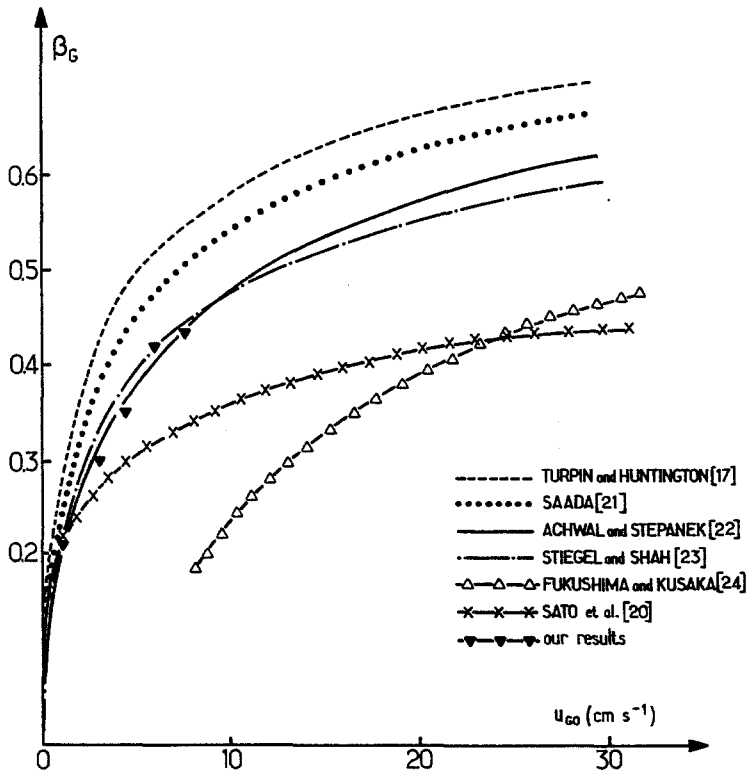

Fig. 5. Variations of the gas hold-up, β_G, with the superficial gas velocity u_{GO} ($L = 6\,kg\,m^{-2}\,s^{-1}$). Comparison with other works [17, 20–24].

Table 2. Experimental conditions for gas hold-up measurements reported by different authors

References	*Bed characteristics (cm)*		*Particle shape*	*Particle size (mm)*	*Void fraction (ε)*	*Flow rates ($kg\,m^{-2}s^{-1}$)*	
	Diameter	*Height*				*Liquid*	*Gas*
[17]	5.1 10.2 15.2	213	Alumina cylinders	7.6 8.23	0.36	Water 6.5–54	Air 2.2×10^{-2}–8.5
[20]	6.5 6.5 6.5		Spheres	12.2 8 5.2		Water	Air
[21]	4.52	40	Spheres (glass)	0.514 0.074 2.064	0.346	Water 1–400	Air 7×10^{-2}–30
[22]	5	105	Ceramic cylinders	6	0.457	Water 4–70	Air 10^{-2}–100
[23]	5	213	Polyethelene cylinders	2.8 × 5.6 3.12	0.41 0.35	Water 3–25	Air 0–0.7
[24]	10 15	63 50	Ceramic spheres	12.7 12.7 25.4		Water + Na_2SO_4 1.5–30	Air 0.03–2.5

$$\beta_G = \left[1 + 4.33 u_{LO}^{-0.433} \left(\frac{u_{LO}}{u_{GO}}\right)^{0.563}\right]^{-1} \quad (5)$$

where u_{LO} and u_{GO} are expressed in $cm\,s^{-1}$. Fig. 6 shows that a maximal deviation of ± 10% exists between the results of this study and the calculated values of β_G using Equation 5.

(c) For a given gas Reynolds number, Re_G, the influence of L ($kg\,m^{-2}s^{-1}$) on β_G is weak in the range of L ($L < 50\,kg\,m^{-2}s^{-1}$) considered in this work (cf. Fig. 7).

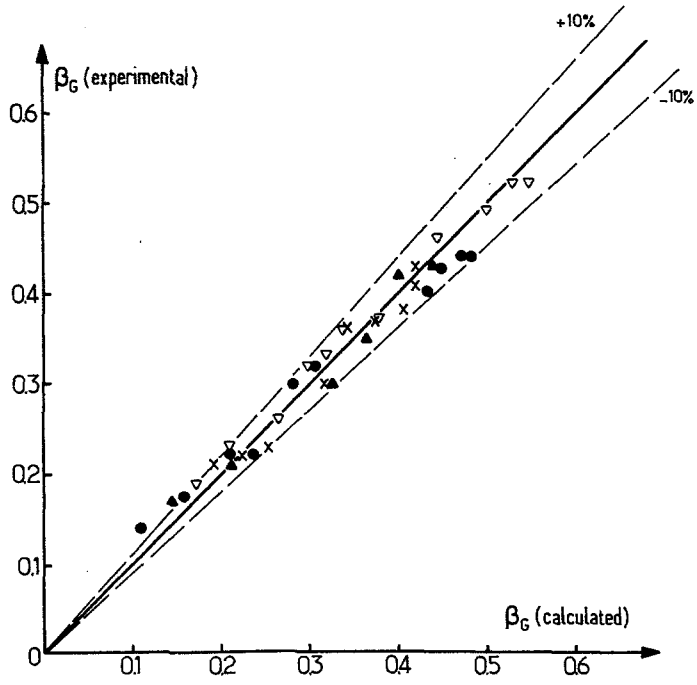

Fig. 6. Comparison of the present gas hold-up results with the correlation of Achwal and Stepanek [22]. $d_p = 4$ mm. Values of L ($kg\,m^{-2}s^{-1}$): ●, 46.7; ▽ 35.0; ×, 10.0; ▲, 6.0.

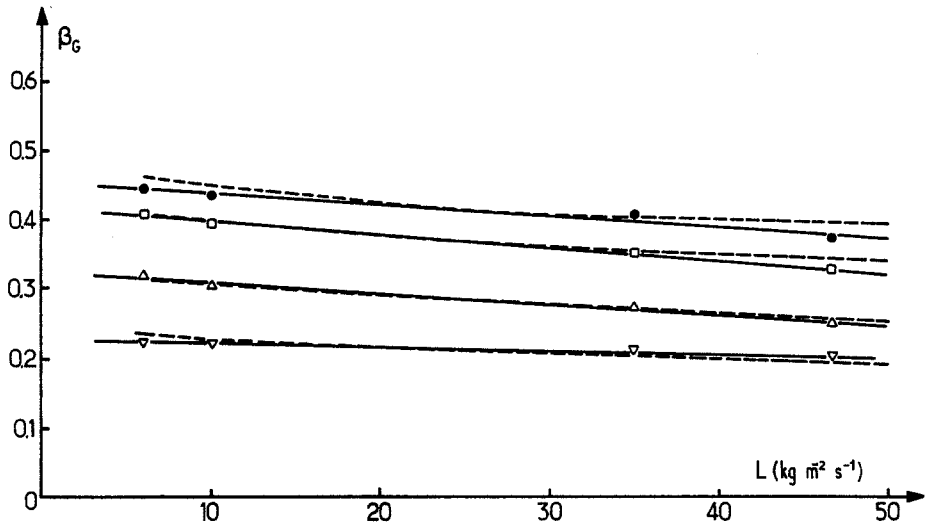

Fig. 7. Influence of the specific liquid flow rate on the gas hold-up β_G (upward co-current flow). Values of Re_G: ▽, 5; △, 10; □, 20; ●, 30. Dashed lines show results of Achwal and Stepanek [22].

3.3. *Mass transfer rates*

The variations of the overall particle to liquid mass transfer coefficient, k'_d, determined from the measurements of the limiting current, with gas and liquid Reynolds numbers are plotted in Fig. 8. Within the experimental precision of the determinations, both active sections are characterized by the same mass transfer rates, showing that the hydrodynamic conditions are fully established inside the column. At small Re_L, k'_d increases sharply with the introduction of a gas flow rate (sometimes a 300% increase compared to the single phase flow) and then the influence of Re_G is less significant. On the contrary, the enhancing effect of the presence of the gas phase is low when the liquid flow is turbulent and becomes undistinguishable at very high liquid flow rates, within the accuracy of the measurements.

At a given liquid Reynolds number, the enhancement of the rates is the result of two effects:

(i) the agitation and turbulence generated by the gas bubbles,

(ii) the increase of the interstitial velocity of the liquid due to decrease of the cross-sectional area available for the liquid flow.

To measure the relative influence of each of these effects, we have reported in Fig. 9a the variations of k'_d with the interstitial velocity $u'_L = u_{LO}/(1 - \beta_G)$ (whereas in Fig. 8 the superficial velocity was used). By comparing Figs 8 and 9a, it is clear that effect (i) is preponderant particularly for small values of L (see the iso-L curves in dotted lines). The same conclusion is deduced from Fig. 9b, which shows the variations of $f = k'_d/k_{d0}$ (ratio of the mass transfer coefficients with and without gas bubbles) with L. The main contribution to the mass transfer enhancement is the turbulence generated by the gas bubbles and not the increase of the interstitial liquid velocity.

4. Experimental results for downward co-current gas–liquid flow

In this configuration of trickle bed, two particle diameters (1 and 4 mm) were used.

4.1. *Flow regimes and pressure drop*

Several flow regimes may be observed: trickling flow, pulsed flow and even spray flow. Their boundaries depend on the respective flow rates of the gas and liquid, the type and dimension of the packing and the physicochemical properties of the fluids [25–30]. For the range of flow rates

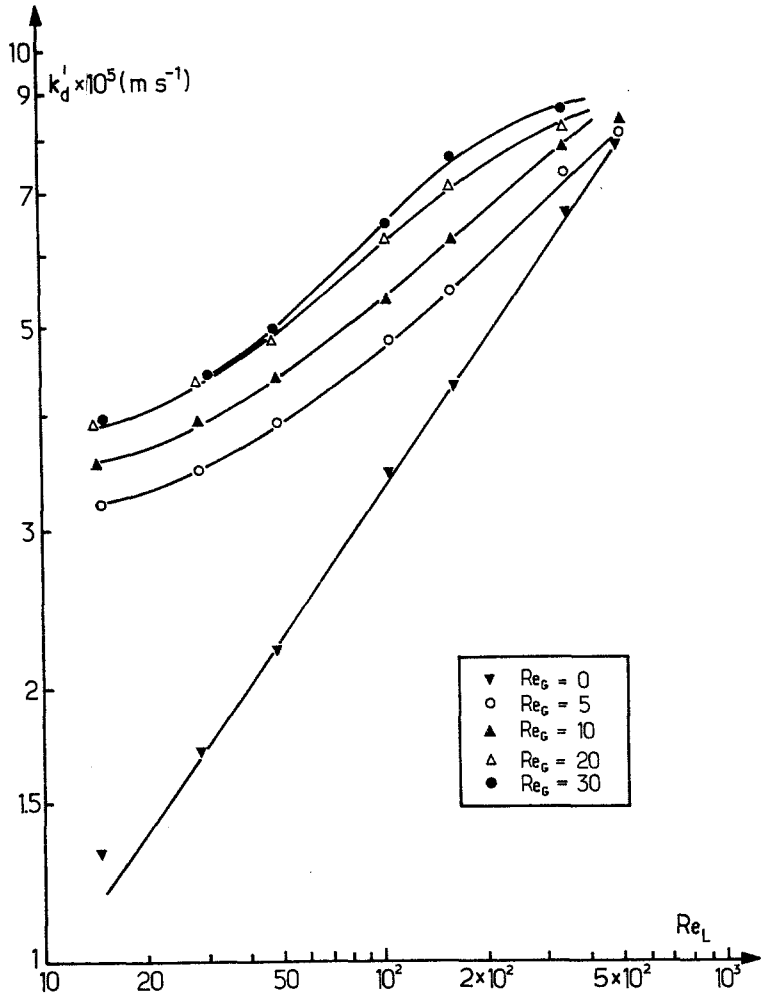

Fig. 8. Variations of the liquid to particle mass transfer coefficient with the gas and liquid Reynolds numbers. Curves $k'_d = f(Re_L)$ for a fixed Re_G.

studied, visual observation has revealed the effective existence of the three flow configurations (even spray flow for $L = 3.4\,\mathrm{kg\,m^{-2}\,s^{-1}}$ and sufficiently high values of G).

These regimes and their boundaries are presented in Fig. 10, in the classical form of $(L/G)\lambda\psi$ versus G/λ where

$$\lambda = \left(\frac{\varrho_L}{\varrho_W}\right)\left(\frac{\varrho_G}{\varrho_{air}}\right)^{0.5} \tag{6}$$

and

$$\psi = \frac{\sigma_W}{\sigma_L}\left[\left(\frac{\mu_L}{\mu_W}\right)\left(\frac{\varrho_W}{\varrho_L}\right)^2\right]^{1/3} \tag{7}$$

The appearance of pulsed flow is in good agreement with the boundary proposed by Charpentier and Favier [28] for non-foaming liquids. The variations of the gas pressure drop with G for different values of L are reported in Fig. 11 as well as the frontier between the trickling and pulsed flow proposed by Midoux *et al.* [31], and are in good agreement with our observations.

4.2. *Liquid overall hold-up* (β_t)

The overall liquid hold-up (static + dynamic) has been measured by means of the residence time distribution technique described above. Fig. 12 presents the variations of β_t with G for different values of L and two particle diameters.

The following conclusions may be drawn.

(a) Over a large range of G, corresponding mainly to the trickle flow regime, (cf. Figs 10, 11), β_t does not depend on the gas flow rate and its

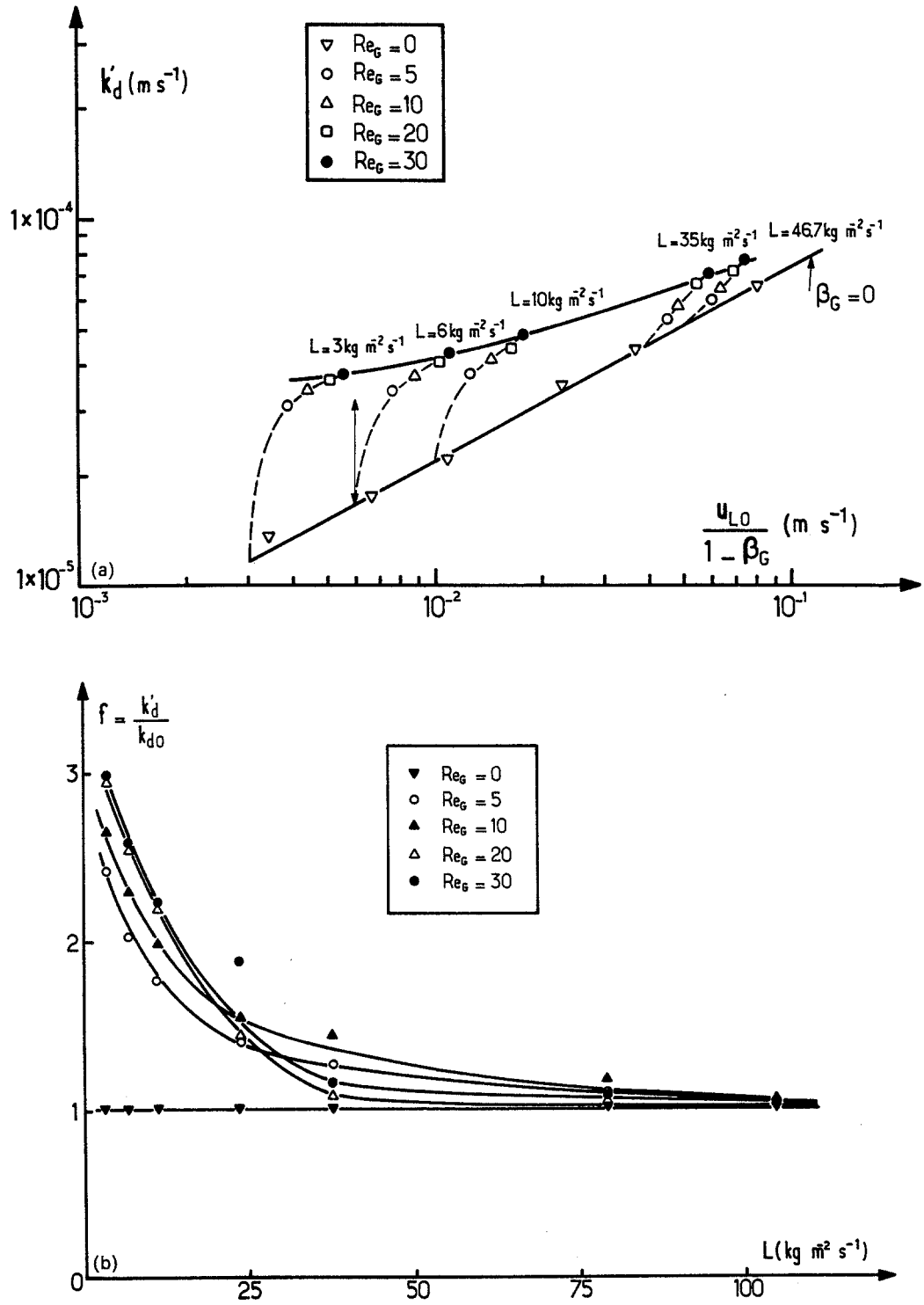

Fig. 9. (a) Variations of k'_d with $u_{LO}/(1 - \beta_G)$ proportional to the liquid interstitial velocity. (b) Experimental variations of the enhancement factor $f = k'_d/k_{d0}$ (ratio of the mass transfer coefficients with and without bubbles) with L.

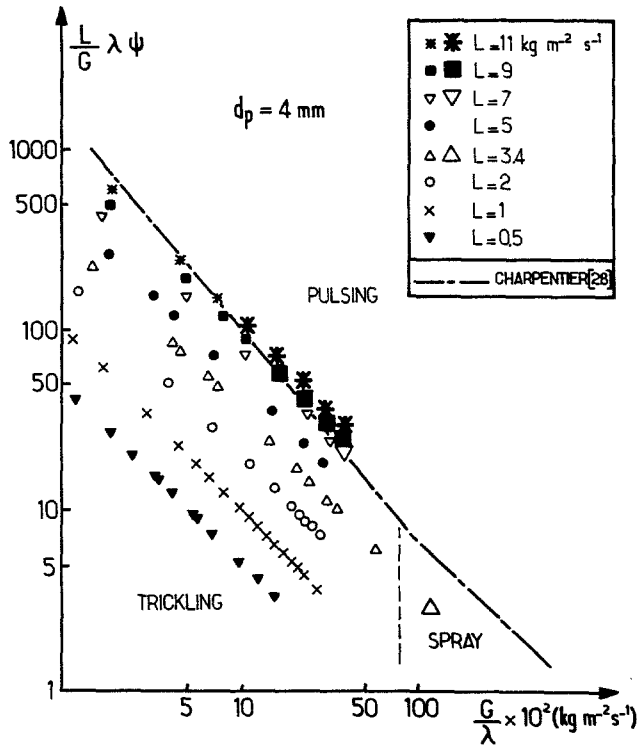

Fig. 10. Hydrodynamic regions observed for downward co-current flow. Comparison with the boundary proposed by Charpentier [28].

value is essentially determined by L. This result may be explained by the fact that in the range considered the interaction between gas and liquid is low.

(b) For larger gas flow rates, β_t seems to decrease as G increases, showing a higher gas–liquid interaction, more especially as L corresponds nearly to the pulsed flow regime.

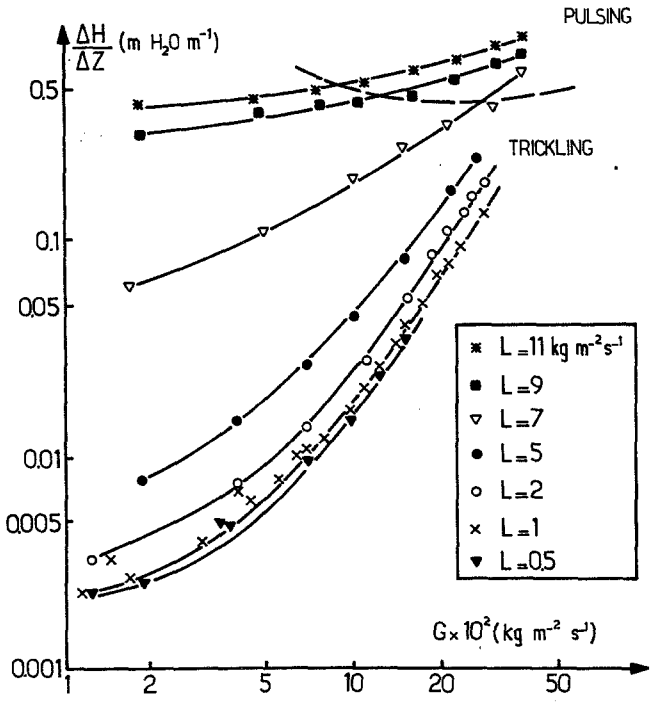

Fig. 11. Experimental variations of the gas–liquid mixture static pressure drop with the gas and liquid specific flow rates (downward flow) when $d_p = 4$ mm.

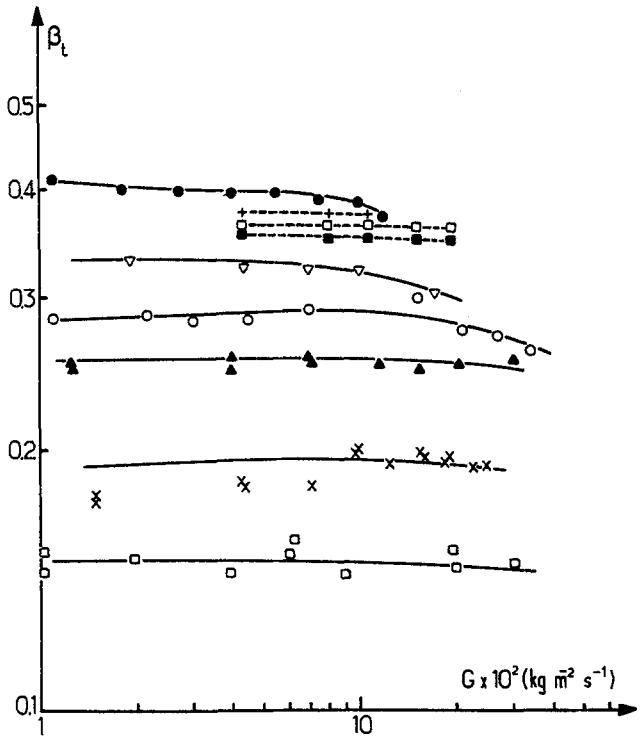

Fig. 12. Experimental variations of the overall liquid hold-up, β_t, with the gas and liquid specific flow rates (downward flow). When d_p = 1 mm, (– – –), values for L (kg m^{-2} s^{-1}) are: ■, 1; □, 2.3; +, 3.5. When d_p = 4 mm (—), values for L (kg m^{-2} s^{-1}) are: □, 0.5; ×, 1; ▲, 2; ○, 3.4; ▽, 5; ●, 6.

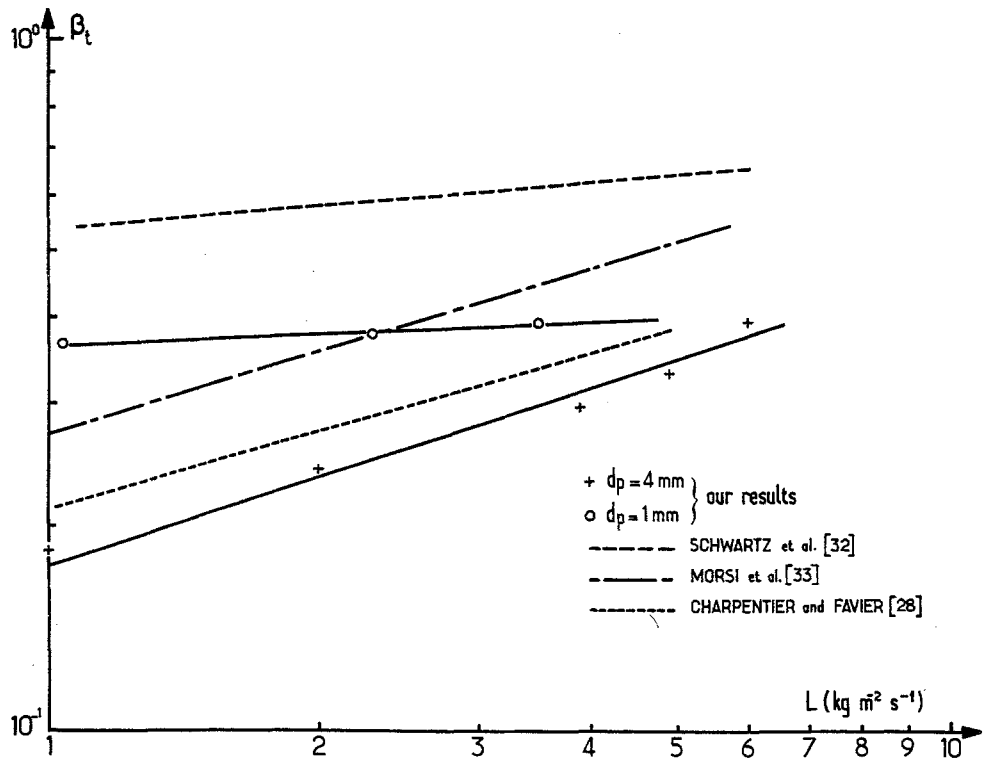

Fig. 13. Comparison of the liquid hold-up results with some literature correlations.

(c) The smaller the particle diameter, the higher the liquid hold-up. For example, for L = 1 kg m^{-2} s^{-1}, β_t ranges from 0.18 to 0.36 when d_p is decreased from 4 to 1 mm.

Comparison of the experimental results with other work [28, 32, 33] for geometrically similar packings is shown in Fig. 13. Except for the correlation proposed by Schwartz *et al.* [32] for smaller particle diameter (d_p = 0.6 mm) leading to higher liquid hold-up, the ranges of variation of β_t are similar although some deviations exist. A precise comparison is difficult due to the difference in experimental conditions, particularly the packing diameter and its wettability.

4.3. *Mass transfer rates*

Contrary to the case of upward co-current flow, for which the fraction, ϕ, of the particle area wetted by the liquid is nearly 100% in the bubble flow regime, the trickle bed configuration, where the gas is the continuous phase, is characterized by an incomplete wetting of the particles. Values of ϕ ranging from 20 to 70% depending on the liquid superficial velocity, u_{LO}, are reported in the literature [34–36]. This is an important difference and, as mentioned in Section 2.2.2, only the product $k_d A_e$ or $k_d \phi$ may be obtained from the experimental limiting current density.

For the particles with d_p = 4 mm, the variations of $k_d A_e$ with G are shown in Fig. 14 for different values of L. In the range of flow rates considered, the gas seems to have no measurable influence on the overall mass flux to the packing; this observation has been mentioned by other authors [37–41]. This weak influence is easily explained if one considers that the trickling regime is a two-phase flow with low gas–liquid interaction. The similar form of the β_t versus G (cf. Fig. 12) compared to the $k_d A_e$ versus G curves is a confirmation of this explanation.

The same result (no influence of the gas phase) has been obtained with smaller particles (d_p = 1 mm). Comparison of the mass transfer rates for both diameters is given in Fig. 15 in the form of the variations of $k_d \phi$ with the superficial liquid velocity, u_{LO}. For $u_{LO} < 5 \times 10^{-3}$ m s^{-1}, $k_d \phi$ is higher for the 1 mm particles. This means that for the same geometrical electrode area, the overall mass flux should be higher with smaller

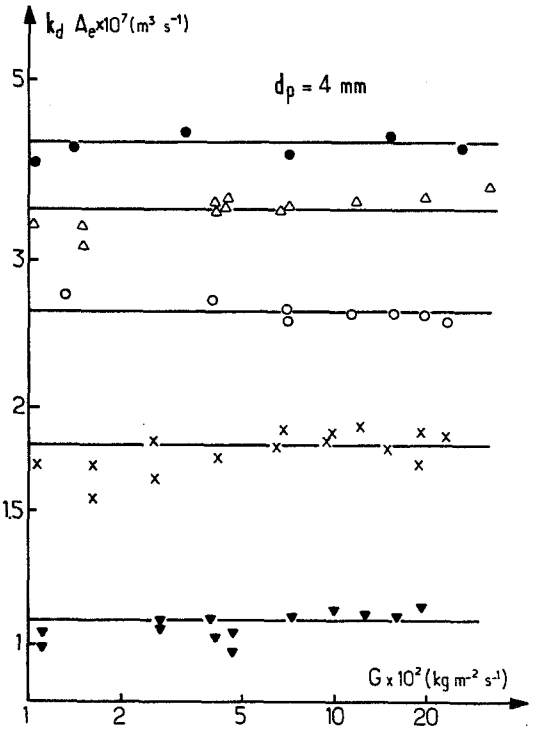

Fig. 14. Experimental variations of the product $k_d A_e$ with the specific liquid and gas flow rates (downward co-current flow). Values of L (kg m^{-2} s^{-1}): ▼, 0.5; ×, 1; ○, 2; △, 3.4; ●, 5.

particles. However, the difference observed in the slope shows the complexity of the hydrodynamic structure of the flow.

In order to compare the results obtained in this work to those of other authors we have used a classical adimensional representation relating the product $Sh\phi Sc^{-1/3}$ to the liquid Reynolds number, Re_L, where

$$Sh\phi = \left(\frac{k_d d_p}{D_L}\right)\left(\frac{A_e}{A_{eg}}\right) \qquad (8)$$

The experimental conditions for the various work cited are reported in Table 3; Table 4 reports the observations and correlations obtained. It is important to note that the methods of determination of the mass transfer rates are generally based on the measurements of the dissolution rate of an organic material weakly soluble in water (benzoic acid, for example). This method has the disadvantage of modifying the particle surface during dissolution.

For the particles with a diameter of 4 mm the

Table 3. Experimental conditions of different authors for overall mass transfer coefficient measurements

Reference	*Bed characteristics (cm)*			*Particle shape*	*Particle size (mm)*	*Void fraction (ε)*	*Experimental technique*	*Fluid nature*	*Flow rates ($kg\,m^{-2}s^{-1}$)*	
	Diameter	*Height*	*Active height*						*Liquid*	*Gas*
[39]	2.58	1.2	1.2	Crushed particle	0.54	0.44	Naphthalene and naphthol dissolution	Air–water	0.118–5.2	0–0.009
		1.2	1.2		1.08	0.44				
		4.1	4.1		2.41	0.43				
[40]	7	53	5.8	Cylinders	3		Benzoic acid dissolution	Nitrogen, helium, argon–water	0.5–25	0–1.6
			10.8		6					
[43]	3.8		9	Cylinders	3		Benzoic acid dissolution	Air–water, water + surfactants	1.6–8.3	0.08–2
	8		15		6					

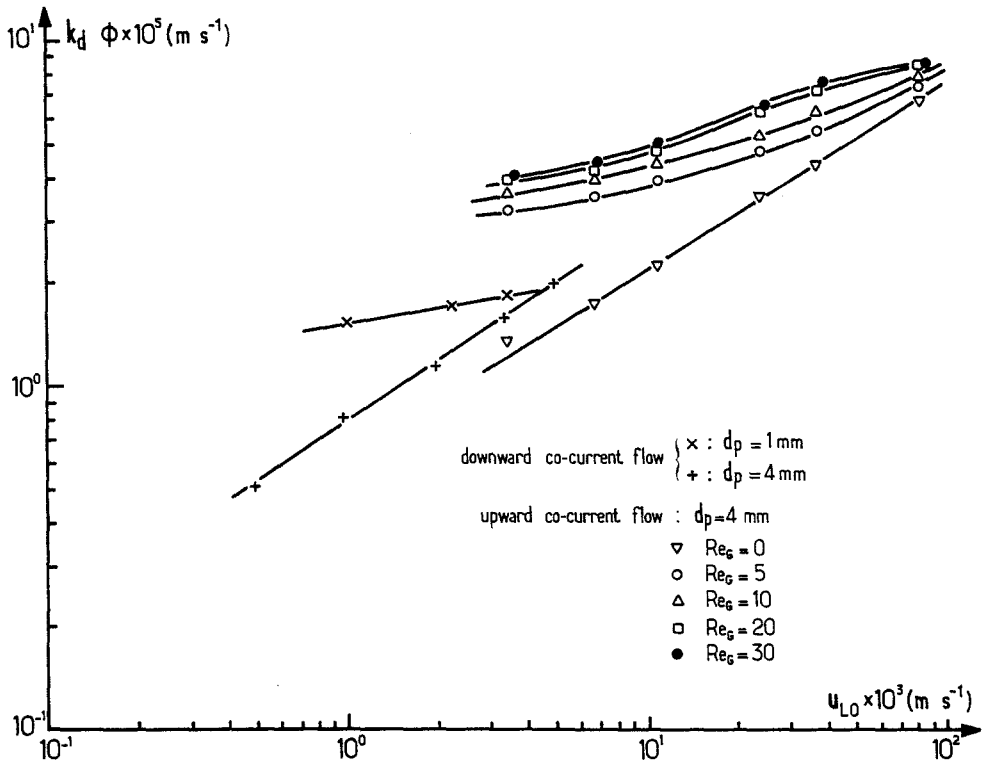

Fig. 15. Influence of the particle diameter on the mass transfer rates for downward and upward co-current gas–liquid flow.

experimental results of this work are in good agreement with the general correlation of Dharwadkar and Sylvester [42] and Goto *et al.* [39] (curves A and B) whose domain of validity is defined by $0 < u_{GO} < 2\,m\,s^{-1}$ and $5 \times 10^{-4} < u_{LO} < 0.25\,m\,s^{-1}$ (cf. Fig. 16). Other correlations show considerable discrepancy in the mass transfer rates which may be attributed to several parameters (packing diameter and form, liquid physicochemical properties, wetting of the packing, method used for the determination).

Table 4. Observations and correlations of different authors for overall mass transfer coefficient measurements (experimental details given in Table 3).

Reference	*Observations and correlations*
[39]	Very low variation of gas flow rate $J_D = 1.31 Re_L^{-0.436}$
[40]	$Sh' Sc^{-\frac{1}{3}} = 0.815 Re_L^{0.802}$ $Re_L < 60$
[42][a]	General correlation, literature compilation $J_D = 1.637 Re_L^{-0.331}$ $0.2 < Re_L < 2400$
[43]	Gas flow rate influence $Sh' Sc^{-\frac{1}{3}} = 2.79 Re_L'^{1.07}$ $Re_L' = \frac{\varrho_L u_{LO}}{a_v \mu_L}$ at $G = 0$

[a] No experimental conditions given — results compiled in literature.

4.4. *Comparison of the mass transfer rates in the two co-current flow configurations*

From the results of sections 3.3 and 4.3 it is possible to compare the overall liquid to particle mass flux for a co-current downward or upward gas–liquid flow. However, before any comparison, the differences between both hydrodynamic structures should be noted. The upward configuration is characterized by a high gas–liquid interaction where the liquid is the continuous phase and the wetting of the particles is almost complete, particularly in the bubble flow regime. The pressure drops of the gas–liquid mixture related to the mechanical energy consumption

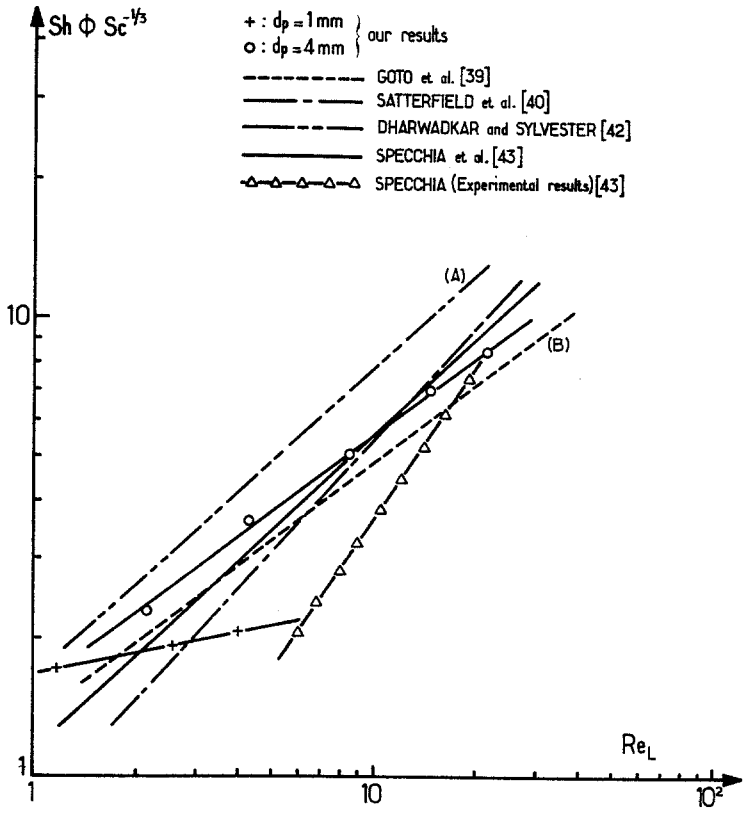

Fig. 16. Adimensional representation of the mass transfer results (downward configuration). Comparison with some correlations of the literature.

are different. The apparent electrolyte conductivity (a parameter not studied in this work) probably presents very different values in each configuration. However, even in the trickle flow regime, where the gas is the continuous phase, it was still possible to obtain a relatively flat plateau of the limiting current density for the mass transfer rate determination.

For the 4-mm nickel particles, Fig. 15 compares the mass transfer rates (parameter $k_d\phi$) obtained in both hydrodynamic configurations for given values of u_{LO}. The comparison is limited to the trickle regime for the downward configuration and to the bubble regime for the upward configuration; the range of velocity u_{LO} is therefore not exactly the same (see the regime boundaries in Figs 4 and 11). From Fig. 15 it appears that the trickle flow leads to higher performances compared to the single phase upflow ($Re_G = 0$, the column is full of liquid); however, the differences observed are relatively small. As seen above, the introduction of a small gas flow rate increases the mass flux for the upward flow sharply, whereas it has no effect in the downward configuration where little gas–liquid interaction occurs. In these conditions, the bubble flow regime yields higher mass transfer rates compared to trickling flow. From the point of view of the mass transfer phenomena and probably also electrolyte conductivity, upward co-current flow gives higher performance. However, for electrochemical processes involving gaseous reactants, where absorption and electrochemical reaction occur, a more complete description would be necessary to compare also the gas–liquid interfacial areas and mass transfer parameters.

5. Conclusions

This paper has shown how important hydrodynamic and mass transfer characteristics of packed beds with co-current gas–liquid flow could be determined by simple electrochemical methods based on the same principle (reduction of ferricyanide ions). Furthermore, from a practical point of view, the introduction of gas bubbles inside an electrolyte flowing upward

through a packed bed electrode is an efficient means of increasing the limiting current densities, particularly at small liquid velocities.

References

[1] A. Storck, M. A. Enriquez, M. Roger and F. Coeuret, *Electrochim. Acta* **27** (1982) 293.
[2] A. Storck, P. M. Robertson and N. Ibl, *ibid.* **24** (1979) 373.
[3] R. Alkire and P. K. Ng, *J. Electrochem. Soc.* **124** (1977) 1220.
[4] C. Oloman and A. P. Watkinson, *J. Appl. Electrochem.* **9** (1979) 117.
[5] *Idem, Can. J. Chem. Eng.* **54** (1976) 314.
[6] C. Oloman, *J. Electrochem. Soc.* **126** (1979) 1885.
[7] N. L. Bathia and A. P. Watkinson, *Can. J. Chem. Eng.* **57** (1979) 631.
[8] G. Kreysa, J. M. Brannen, W. Kochanek and G. Linzbach, *J. Appl. Electrochem.* **5** (1985) 639.
[9] G. H. Sedahmed, *ibid.* **8** (1978) 399.
[10] D. J. Economou and R. C. Alkire, *J. Electrochem. Soc.* **132** (1985) 601.
[11] N. Ibl, R. Kind and E. Adam, *An. Quim.* **71** (1975) 1008.
[12] L. Sigrist, O. Dossenbach and N. Ibl, *Int. J. Heat Mass Transfer* **22** (1979) 1008.
[13] N. Ibl, *Electrochim. Acta* **24** (1979) 1103.
[14] Gh. Delaunay, A. Storck, A. Laurent and J. C. Charpentier, *Ind. Eng. Chem. Process. Des. Dev.* **19** (1980) 514.
[15] F. Hine, 'Electrolytic Gas Evolution', Paper presented at the Annual Meeting of the International Society of Electrochemistry, Berkeley, USA, August 1984.
[16] R. Aris, *Chem. Eng. Sci.* **9** (1939) 266.
[17] J. L. Turpin and R. L. Huntington, *AIChE J.* **13** (1967) 1196.
[18] Pittsburgh Energy Research Center (PERC) Quarterly reports (1976).
[19] V. Specchia, S. Sicardi and A. Gianetto, *AIChE J.* **20** (1974) 646.
[20] Y. Sato, T. Hirose and T. Ida, *Kagaku Kogaku* **38** (1974) 543.
[21] M. Y. Saada, *Periodica Polytech. Chem. Eng.* **19** (1975) 317.
[22] S. K. Achwal and J. B. Stepanek, *Chem. Eng. J.* **12** (1976) 69.
[23] G. J. Stiegel and Y. T. Shah, *Ind. Eng. Chem. Process. Des. Dev.* **16** (1977) 37.
[24] S. Fukushima and K. Kusaka, *J. Chem. Eng. Jap.* **12** (1979) 296.
[25] O. Baker, *Oil Gas J.* **53** (1954) 185.
[26] V. W. Weekman and J. E. Meyers, *AIChE J.* **10** (1964) 951.
[27] Y. Sato, T. Hirose, F. Takahashi, M. Toda and Y. Hashiguchi, *J. Chem. Eng. Jap.* **6** (1973) 315.
[28] J. C. Charpentier and M. Favier, *AIChE J.* **81** (1975) 1213.
[29] V. Specchia, A. Rossini and G. Baldi, *Chem. Eng. Sci.* **32** (1977) 515.
[30] A. Gianetto, G. Baldi and S. Sicardi, *AIChE J.* **24** (1978) 1087.
[31] N. Midoux, M. Favier and J. C. Charpentier, *J. Chem. Eng. Jap.* **9** (1976) 350.
[32] J. G. Schwartz, E. Weger and M. P. Dudukovic, *AIChE J.* **22** (1976) 894.
[33] B. I. Morsi, N. Midoux and J. C. Charpentier, *ibid.* **24** (1978) 357.
[34] S. Sicardi, G. Baldi, V. Specchia, I. Maggarino and A. Gianetto, *Chem. Eng. Sci.* **36** (1981) 226.
[35] X. Onda, E. Sada and Y. Murase, *AIChE J.* **5** (1959) 235.
[36] R. Krauze and M. Serwinski, *Ingyniera Chemiczna* **1** (1971) 415.
[37] T. Hirose, Y. Mori and Y. Sato, *J. Chem. Eng. Jap.* **9** (1976) 220.
[38] S. Goto and J. M. Smith, *AIChE J.* **21** (1975) 706.
[39] S. Goto, G. Levec and J. M. Smith, *Ind. Eng. Chem. Process. Des. Dev.* **14** (1975) 473.
[40] C. N. Satterfield, M. W. Van Eek and G. S. Bliss, *AIChE J.* **24** (1978) 709.
[41] J. A. Ruether, C. Yang and W. Hayduk, *Ind. Eng. Chem. Process. Des. Dev.* **19** (1980) 103.
[42] A. Dharwadkar and N. D. Sylvester, *AIChE J.* **23** (1977) 376.
[43] V. Specchia, G. Baldi and A. Gianetto, *Ind. Eng. Chem. Process. Des. Dev.* **17** (1978) 362.